THE SEISMIC NONLINEAR STATIC ANALYSIS COMPARISON OF HIGH-RISE BUILDING USING DIFFERENT FRAME SYSTEM CONFIGURATION

Armin NAIBAHO
Master, Civil Engineering Department, Management and Construction Engineering, State Polytechnic of Malang, Malang, Jawa Timur, Indonesia,
e-mail: armin.naibaho@polinema.ac.id

Taufiq ROCHMAN
Professor, Head of Structural Engineering Laboratory, Civil Engineering Department, State Polytechnic of Malang, Malang, Jawa Timur, Indonesia,
e-mail: taufiq.rochman@polinema.ac.id

Abstract. The dimensions and arrangement of columns have a significant impact on the seismic behavior of a structure. The objective of this paper is to ascertain the appropriate dimensions and configuration of columns for a building utilizing a frame system and framed tube system. Various column sizes and configurations were utilized to model four different types of buildings. The pushover analysis method was employed to determine the deformation capacity. The results obtained from the pushover analysis, indicate that the drift ratio for each building model remains below the prescribed 2% drift limit. The fourth building model, known as the framed tube system, exhibits the lowest drift ratio among the models, measuring at 0.81%. Upon reviewing the budget plan, it is evident that the second model building exhibits the lowest cost, displaying a notable disparity of 20.98% in comparison to the fourth model building, which boasts the highest cost. After considering both structural performance and budgeted cost, it is determined that the framed tube structural system is the optimal configuration.

Key words: column size, frames structural system, framed tube system, pushover analysis, story drift ratio.

1. Introduction

The process of urbanization will lead to a heightened demand for spatial resources within urban areas, thereby causing a progressive scarcity of favorable land. One of the defining features of urbanization is the alteration of land use for residential construction. Numerous studies have identified positive outcomes in terms of policy recommendations for fostering a beneficial relationship between urbanization and economic growth. Additionally, these studies have emphasized the importance of promoting the development of new environmentally sustainable urban areas and ecosystems (Liang and Yang, 2019; Reynolds *et al.*, 2019). More than 50% of the reported cases demonstrated the simultaneous occurrence of changes in land cover and

socioeconomic processes (Shaw *et al.*, 2020; Yu, 2021). Hence, adopting a vertical or high-rise construction approach emerges as a potential solution to address this challenge. Nevertheless, Indonesia's geographical location renders it prone to seismic activity, leading researchers to conduct numerous studies on the subject. One such study focuses on the characterization of landslides triggered in Padang, Indonesia. The findings of this research offer valuable insights that can aid in predicting the specific attributes of landslides that may be triggered by future earthquakes in the region (Umar *et al.*, 2014). Previous studies have examined the significance of seismic-induced environmental effects in seismic sequences, revealing that these effects provide additional information to complement conventional reports on intensity and structural failures (Ferrario, 2019), post-earthquake damage maps play a crucial role as a valuable tool in the development and implementation of hazard mapping and mitigation strategies. The objective is to minimize the number of casualties and ascertain the optimal course of action for subsequent design and advancements (Syifa *et al.*, 2019; Jena *et al.*, 2020).

The investigation of the extent of ground failure and infrastructure damage resulting from the event, with a specific focus on the Jono-Oge region where the flow distance was most significant (Hazarika *et al.*, 2021), is a key area of interest for researchers as a precautionary measure. It is important to note that the geological phenomena of pumice fall, weathering, and undercutting, which contribute to such occurrences, are not exclusive to the affected area but rather are prevalent in numerous volcanic regions, enables the identification of regions susceptible to seismic-triggered debris avalanches (Hosobuchi *et al.*, 2021), as a result of the convergence of the three major tectonic plates on Earth, namely the Australian plate, the Eurasian plate, and the Pacific plate. The present situation poses a noteworthy construction obstacle.

In regions characterized by substantial seismic activity, the utilization of reinforced concrete skeleton systems, also known as reinforced frame systems, is commonly employed as a means of structural support during earthquakes. It is worth noting that the type of soil plays a crucial role in the interaction between the soil and the structure (Moosavi *et al.*, 2022) including dynamics circumstances were investigated (Zhang and Far, 2022). The efficacy of the system is showcased through a comparative analysis of traditional and decoupled infilled reinforced concrete (RC) frames subjected to both individual and combined loading scenarios (Marinkovic and Butenweg, 2019) in the case of tall buildings, the elevation of the structure is augmented to leverage the internal tube as a primary mechanism for counteracting gravitational loads, as opposed to lateral loads. This strategic approach enables the building to achieve a reduced weight without compromising compliance with practical and design code prerequisites (Sarcheshmehpour *et al.*, 2020). Another researcher has observed the migration of cracks from longitudinal beams to transverse beams along the path of the corner zones of the drilled slabs. Consequently, the beam-column frame node exhibited partial preservation of its structural integrity, specifically in terms of strength and stiffness (Sococol *et al.*, 2022), multiple earthquake effects can exert a substantial influence on the behavior of reinforced concrete structures in manners that are not easily anticipated

through basic analysis. The discovered results have the potential to inform the development of design methodologies that yield appropriate levels of structural safety for systems exposed to multiple seismic events, aligning with existing earthquake engineering design codes (Abdelnaby and Elnashai, 2014) such as (Shooli *et al.*, 2019; Zhang and Tian, 2019; Sattar, 2018; Muljati *et al.*, 2017; Zameeruddin and Sangle, 2016). Various methods of structural support have garnered significant interest in the context of tubular construction featuring frame compartments. The framed tubular system is widely recognized as the most frequently employed method (Zhang and Far, 2022; Emre, 2021; Shariati *et al.*, 2020; Rahgozar, 2020; Ali and Moon, 2018). The external framework of the tube exhibits significantly larger rigidity compared to previous tubular systems (Fu, 2018).

The column, possesses a high level of complexity owing to its ability to withstand and distribute axial, sliding, and moment forces, especially when subjected to seismic conditions (Rochman *et al.*, 2020). Columns are specifically engineered to withstand higher moments in comparison to beams, as they adhere to the principle of strong column-weak beam (Shukla and Dalal, 2017), the utilization of performance-based plastic design has been investigated by researchers (Dalal and Dalal, 2021) and (Ouyang *et al.*, 2022). The occurrence of a structure collapse may arise due to the failure of one or multiple columns, despite the investigation conducted to prevent such incidents (Dalal and Dalal, 2021; Razavi and Gholizadeh, 2021). Based on the information, it is imperative to consider (Muljati *et al.*, 2015) the potential complete structural collapse of buildings in earthquake-prone areas with established seismic characteristics (Imran *et al.*, 2021; Zameeruddin and Sangle, 2016; Lin *et al.*, 2019) when design for future.

Based on that research, it is imperative to anticipate the complete structural failure of buildings located in earthquake-prone areas with well-documented behavior, to inform the design of future structures. The objective of this study is to reduce the fundamental period of reinforced concrete frame structures during the design phase. The conventional structure exhibits a heightened vulnerability to collapse due to its greater susceptibility to incurring losses associated with building collapse (Arroyo *et al.*, 2017). The structural moments remain in an elastic state (Sococol *et al.*, 2021) until their transition into a nonelastic state, achieved by identifying the appropriate column configuration for structural frames and framed tubes.

2. Methods

First, it is necessary to examine the configuration column. The study places emphasis on four alternatives, comprising of two building models employing a structure frame system and two building models utilizing a structure framed tube system. The data utilized in this research study is comprised of the following information. The separation being referred to is an integral component of the analytical model. The subsequent stage involves the development of the initial design for the four building models, including the determination of the mass of each structural system. The variable has been set to a constant value. Next, employ the methods of analysis, gravitational, or seismic loading to proceed.

The preceding analysis can be simulated using the SAP2000 software to gain

insights into the resultant forces. The obtained analysis results will be utilized in the process of designing reinforcement beams and columns for every building model. Subsequently, reinforcement beams and columns will be incorporated into the pushover analysis, aiming to assess the extent to which the structural deformability affects the sizing of the columns. The evaluation of performance using the ATC-40 capacity method will involve utilizing the pushover analysis output in the form of a curve capacity.

When comparing the four building models, the cost estimation is determined by considering factors such as the volume of concrete, the weight of iron, and the structural elements of large formwork beams and columns. Additionally, the performance of these models is evaluated. Then architectural designs will encompass four distinct building models, namely A, B, C, and D. Models A and B represent structure-framed systems, whereas models C and D reflect structure-framed tube systems. The four architectural models exhibit variations in terms of their configuration and size, while adhering to identical technical building specifications. To ensure that the seismic energy impact on a building is consistent, it is a must for each structural model, to possess an equivalent mass.

2.1 Determination of columns dimension and building mass in each model

The material data, dimensions and mass equalization were assessed for each building structure system, specifically model A in comparison to model B (frame system), and model C in comparison to model D. This evaluation was conducted based on the structural configuration depicted in Fig. 1.

Table 1. Data of materials (Source: Authors).

Data and brands	Yield Strength (MPa)	Ultimite Strength (MPa)	E (MPa)
Concrete (Jaya Mix)	-	fc' = 35	27,806
Steel main (Krakatau Steel)	400 (BJ55)	570 (BJ55)	200,000
Steel trans. (Krakatau Steel)	240 (BJ37)	370 (BJ37)	200,000

The material data described in Table 1 and column dimensions declared in Table 2 utilized are solely intended for illustrative purposes and have been derived from the practical building methodology employed in the field.

Table 2. Preliminary column's dimension design for model A to D (Source: Authors).

Building model	Column type	b (m)	h (m)	Mass (kN)	Total mass (kN)
Model A	K1-A	0.8	0.8	1317.1	1317.1
Model B	K1-B	1.0	1.0	1317.1	1317.1
Model C	K1-C	0.6	0.6	1079.0	1473.8
	K2-C	0.73	0.73	394.8	
Model D	K1-D	0.7	0.7	1331.1	1729.5
	K2-D	0.6	0.6	398.4	

The initial design of this column did not account for any applied loads. Therefore, the dimensional analysis of the column elements, as an earthquake-resistant structure in accordance with SNI 2847:2019, is only evaluated based on the first two parameters. These parameters specify that the shortest dimension of the column cross-section should be no less than 300mm, and the ratio of the shortest dimension to the perpendicular dimension should not be less than 0.4 ($b/h>0.4$). In the initial phase of beam design, the height of the beam is established in relation to the span length, while the width is iteratively adjusted in order to achieve a balanced distribution of mass across each model of the structure such accomplished in Table 3 and mass in Table 4.

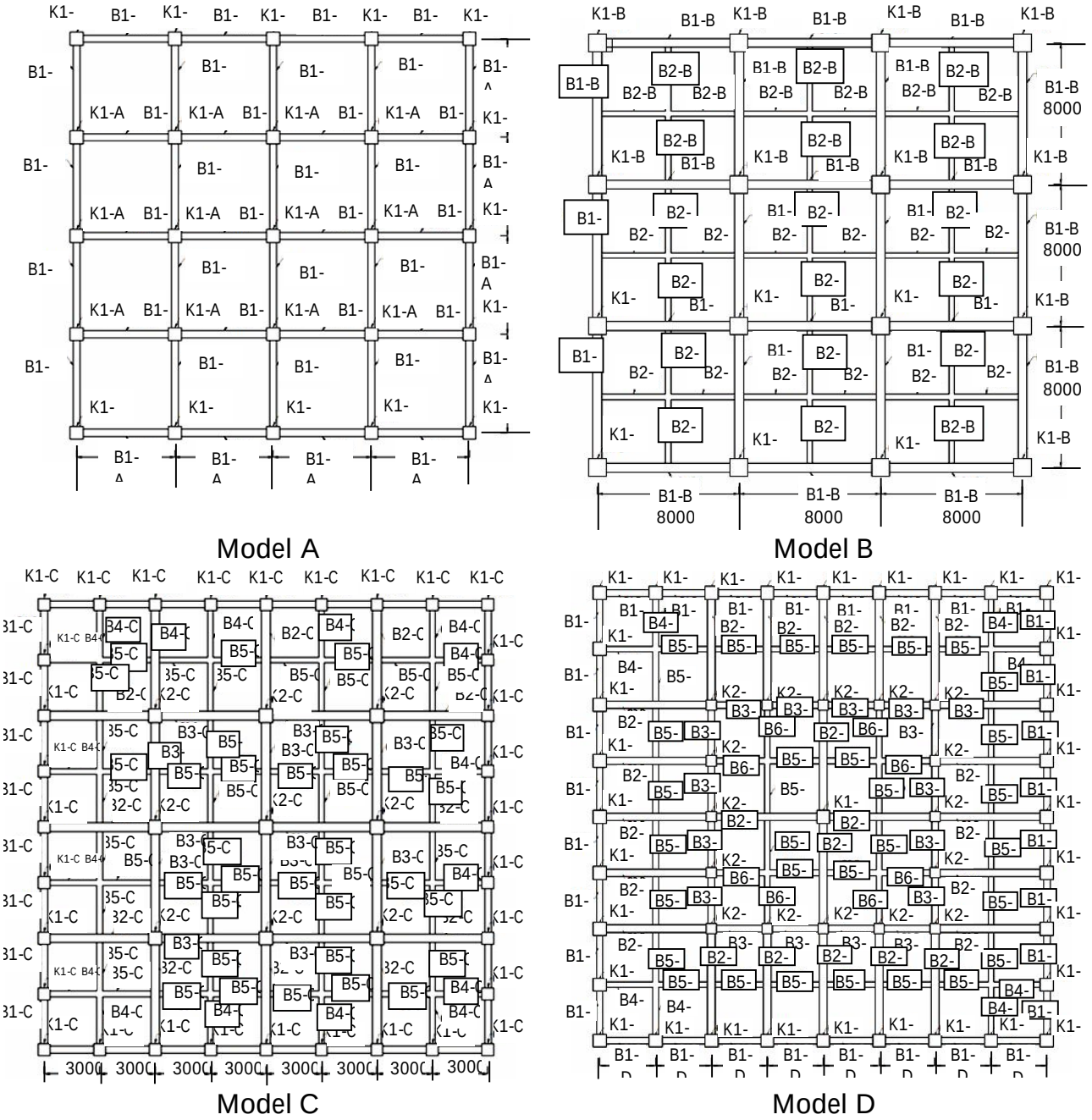

Fig. 1. Structural system configuration of each building model.

In this study, the slab or plate elements for all building models have been uniformly designed with identical thicknesses to ensure that the mass of the plates remains consistent across all building models, as depicted in Table 5 and modeling layout of all building models depicted in Fig. 2.

2.2 Dead Loads and Live Loads

The design structures are loaded according to the specifications outlined in the SNI 1727:2020 standard code such described in Table 6 and 7. This standard provides the minimum design loads and criteria for building structures and other types of structures, including dead loads, live loads and the illustration of the load distribution depicted in Fig. 3.

2.3 The seismic Load

1) Determine seismic acceleration parameter
To get a more accurate value, one can search for it by accessing the Indonesian Spectra Design Application via the website address http://rsa.buatkarya.pu.go.id/2021 such as:

Table 3. Preliminary beam's dimension design for model A to D (Source: Authors).

Building model	Beam type	b (m)	h (m)	Mass (kN)	Total mass (kN)
Model A	B1-A	0.4	0.7	1472.5	1860.32
	B2-A	0.3	0.4	387.78	
Model B	B1-B	0.5	0.8	1481.8	1862.8
	B2-B	0.3	0.4	381.0	
Model C	B1-C	0.4	0.5	300.5	1912.0
	B2-C	0.5	0.7	458.28	
	B3-C	0.5	0.7	454.4	
	B4-C	0.4	0.5	170.6	
	B5-C	0.4	0.5	528.17	
Model D	B1-D	0.4	0.5	302.9	1656.1
	B2-D	0.4	0.6	771.3	
	B3-D	0.4	0.5	161.4	
	B4-D	0.3	0.5	67.3	
	B5-D	0.3	0.5	284.0	
	B6-D	0.3	0.5	69.2	

Table 4. Mass equalization of columns and beams of 4 models (Source: Authors).

Building model	Column's mass (kN)	Beam's Mass (kN)	Total mass (kN)
Model A	1317.1	1860.3	3177.4
Model B	1317.1	1862.8	3179.9
Model C	1473.8	1912.0	3385.8
Model D	1729.5	1656.1	3385.6

Table 5. Preliminary slab's dimension design for model A, B, C, and D (Source: Authors).

Floor	type	Thickness (m)	Total mass (kN)
1 – 29	S1	0.12	1625.7
25 (roof)	S2	0.11	1490.23

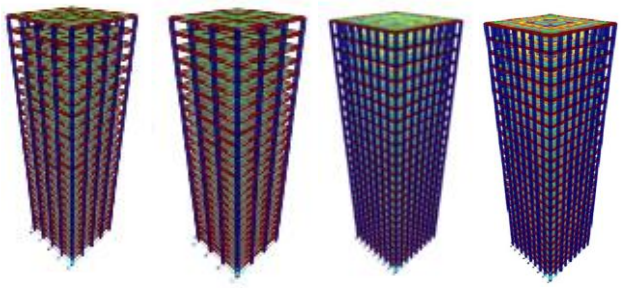

Fig. 2. Modeling Layout Design of : a) Model A, b) Model B, c) Model C, d) Model D.

The parameters Ss (bedrock acceleration in a short period) and S_1 (bedrock acceleration in a 1 second period) must be determined respectively from the 0.2 second and 1 second acceleration spectral responses in the seismic ground motion maps in Fig. 4a) and Fig. 4b) with the possibility 2% is exceeded in 50 years (MCER, 2% in 50 years), and is expressed in decimal numbers relative to gravitational acceleration (SNI 1726:2019 code).

Table 6. Dead loads (Source: Authors).

Floor Stories	Total self-weight and dead load (kN)			
	Model A	Model B	Model C	Model D
1st	6,937.3	6,937.7	7,224	7,351.7
2 -24	138,189.3	138,245.9	142,982.4	142,977.3
25th	4,601.6	4,604	4,731.6	4,603.5
Total	149,728.1	149,789.7	154,938.1	154,932.5

Table 7. Live loads (Source: Authors).

Floor Stories	Total Live Load (kN)			
	Model A	Model B	Model C	Model D
1 -24	33,177.6	33,177.6	33,177.6	33,177.6
25th	550	553	553	553
Total	33,737.6	33,730.6	33,730.6	33,730.6

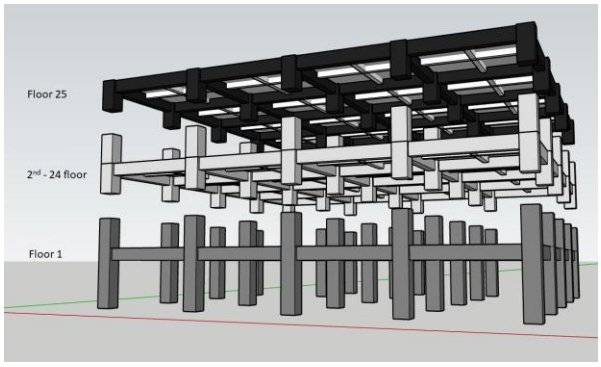

Fig. 3. Illustration on the load distribution in Table 6 and Table 7.

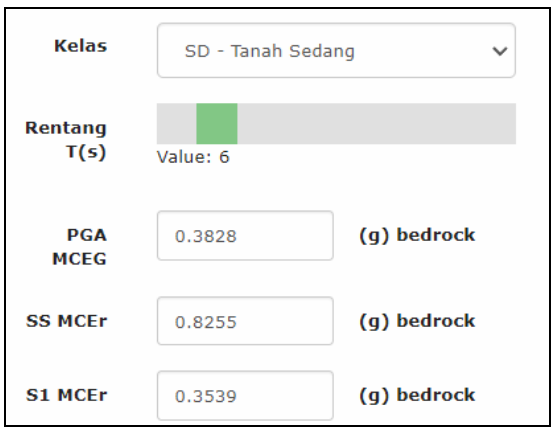

Fig. 4. Medium soil, T=6, PGA=0.38g, Ss=0.8255, S_1=0.3539 from the website

The direct access of spectrum response design for seismic analysis is facilitated through the Indonesia Ciptakarya PU application design. The analysis of the location area studies, specifically Bukit Darmo Golf Surabaya, resulted in Fig. 4, (from website) and Fig. 5 a) and Fig. 5 b) form the seismic map, the values: S_S = 0.8255 and S_1 = 0.3539. The risk category for constructing office buildings falls under category II, while the seismic importance factor (Ie) is assigned a value of 1.0. It is postulated that the land is situated on soil conditions of moderate quality (SD), leading to a classification of SDC (Seismic Design Category) of D. Fig. 4c) illustrates the correspondence response spectrum diagram for Surabaya area.

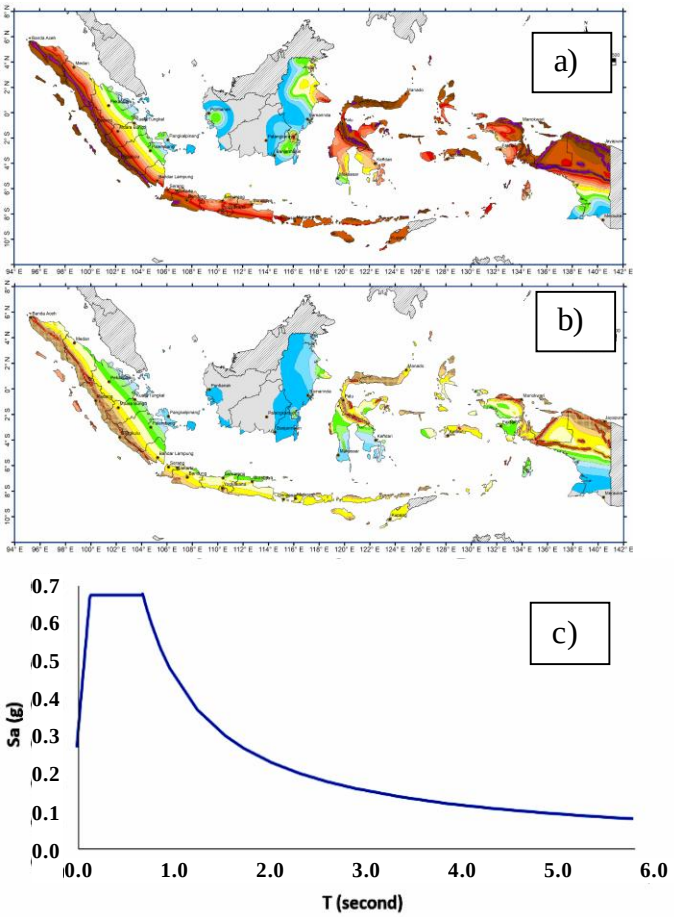

Fig. 4. a) Acceleration Spectra 0.2 Second (S_S) Short Period Response Map in Bedrock (SB) for a Probability of Exceeding 2% in 50 Years with 5% damping; b) Acceleration Spectra 1 Second (S_1) Response Map in Bedrock (SB) for a Probability of Exceeding 2% in 50 Years with 5% damping; and c) Response spectrum diagram for Surabaya with 5% damping according SNI-1726:2019.

The PGA research (Susilo and Adnan, 2013) showed that for the acceleration of bedrock at T=0 second (PGA), T=0.2 seconds (short period) and T=1 seconds (long period) have values between 0.09 g - 0.29 g (PGA), 0.19 g - 0.61 g, and 0.06 g - 0.29 g respectively.

2) Determine the Site Coefficient
Subsequently, the categorization of the site and the determination of S_S and S_1 values are employed to calculate the seismic amplification factors for short 0.2 sec. period (Fa) and 1 sec. period (Fv) in SNI-1726:2019. Given an SS value of 0.8255 and an SD site class, the corresponding Fa value is 1.1698. Similarly, with an S1 value of 0.3539 and for an SD site class, the corresponding Fv value is 1.9461.

3) Determine the Seismic Acceleration Spectral Response Parameters
The determination of acceleration spectral response parameters in short periods (S_{MS}) and 1 sec. periods (S_{M1}), which are adjusted for the site classification effect as:
a) S_{MS} = Fa . SS = 1.1698 (0.8255) = 0.966 g
b) S_{M1} = Fv . S1 = 1.9461 (0.3539) = 0.689 g

4) Determine Design Spectral Acceleration Parameters
The design spectral acceleration parameters for short period 0.2 sec. (S_{DS}) and 1 sec. (S_{D1}) can be computed using:
a) S_{DS} = 2 / 3 . S_{MS} = 2 / 3 (0966) = 0.644 g
b) S_{D1} = 2 / 3 . S_{M1} = 2 / 3 (0.689) = 0.459 g
5) Determine the Seismic Design Category
To proceed, it is necessary to ascertain the seismic design category by utilizing the values of the design spectral acceleration parameter and their risk categories as:
a) The building has an S_{DS} value of 0.644 g and is classified as risk category II. It falls under seismic design category D because the S_{DS} value is higher than the threshold of 0.50 g.
b) The building is classified as seismic design category D due to its S_{D1} value of

0.459 g, which surpasses the threshold of 0.20 g, placing it in risk category II.

6) Determine the Design Response Spectrum and fundamental period,
$T_S = S_{D1} / S_{DS} = 0.644 / 0.459 = 0.713$ second
$T_0 = 0.2(S_{D1} / S_{DS}) = 0.2\ (0.644 / 0.459) = 0.143$ sec
Then, make the curve
For $T < T_0$, then $S_a = S_{DS}\ (0.4 + 0.6(T / T_0))$
For $T_0 \leq T \leq T_S$, then $S_a = S_{DS}$
For $T \geq T_S$, then $S_a = S_{D1} / T$
And then resulted in response spectrum diagram as depicted in Fig. 4c).

7) Determine the structural system,
The structural system employed is SMRF (Special Moment Resisting Frame), where the values of the parameters are R = 8, Cd = 3, and Ωo = 5.5, as determined from previous data.

8) Determine the fundamental period
As SNI-1726:2019 code, buildings classified as moment-bearing concrete frames, such as model A and model B (frame system), have values of $C_t = 0.0466$ and x = 0.9. Model C and Model D buildings, which are framed tube systems, are classified within the broader category of all other structural systems. Therefore, they are assigned values of $C_t = 0.0488$ and x = 0.75. Subsequently, these two coefficients are employed to compute the precise value of the fundamental period of the structure. The maximum allowable value for Ta should not surpass the product of Cu and Ta, where Cu is a coefficient with a value of 1.4 according to SNI-1726:2019.

Model A and B can be represented by:
$T_a = C_t \cdot h^x$
$T_a = 0.0466 \cdot (87.5)^{0.9} = 2.607$ secs
$T_{max} = C_u \cdot T_a = 1.4\ (2.607) = 3.65$ secs
Model C and D can be represented by:
$T_a = 0.0488 \cdot (87.5)^{0.75} = 1.396$ secs
$T_{max} = 1.4\ (1.396) = 1.96$ secs

The SAP2000 v21.0.2 program was used to conduct a structural analysis, resulting in the determination of the fundamental period value Tc for each building model. These values are presented in Table 8.

Table 8. Fundamental period of each model

Fundamental Period, T_c (second)			
Model A	Model B	Model C	Model D
3.986	4.643	4.011	3.797

9) Determining modal response parameters
According to the specifications outlined in SNI 1726:2019, specifically in Article 7.9.1.2, the parameters for evaluating forces, such as deviations between levels, bearing forces, and force elements, need to be determined using specific quantities. In this case, the calculation involves:
Ie / R = 1.0 / 8 = 0.125 g (0.98) = 1.226 seconds
The parameter inputted into SAP2000 is 1.226 seconds.

3. Results and Discussion

The analysis procedure performed for the evaluation of a 87.5 m height reinforced concrete buildings, as specified in the SNI 1726:2019 code, is the dynamic spectrum response variety analysis. The regulation of the participation mass is a crucial factor, as indicated in Table 9.

3.1 The number of modal responses

The analysis should encompass a sufficient range of variables to ensure that the participation mass in each horizontal orthogonal direction from the model's reviewed responses is at least 90% of the actual mass. Based on the data presented in Table 9, it can be observed that the 80th mode satisfies the requirement of achieving a minimum participation rate of 90%.

All four building models adhere to the same set of procedures, ensuring that each model fulfills the requirement of achieving a minimum of 90% participation on the 80th mode.

Table 9. Response mode and mass participation on Model B (Source: Authors).

Mode	Sum of UX	Sum of UY
1	0.00085	0.77818
10	0.91462	0.93526
20	0.96301	0.962
30	0.97217	0.97217
40	0.97691	0.97691
50	0.98073	0.98073
60	0.98073	0.98073
70	0.98073	0.98073
80	0.98073	0.98073

3.2 Determining combined response parameters

Once the time participation has been completed, the control method summation is calculated for the selected model in SAP2000, and the resulting outputs are presented in Table 9. The mean deviation between consecutive time-shakes in modes 1 to 80, when compared to the natural mode, is approximately 4%. This suggests that the existing summation method provides sufficient variability.

The method combination squared complete (CQC) is applicable in this case due to the observed difference of 15%. Uniform procedures are adhered to for all building models. The implementation of the running was carried out after the completion of preliminary design and analysis of the structures and their corresponding loading conditions.

Table 10. Control of mode summation method.

Mode	Period	Differences (%)
1	4.64	0
2	4.64	20
3	3.71	60
4	1.497	0
5	1.497	19
…	…	…
80	0.125	0

3.3 Modifying Scale Factor for Response Spectrum Analysis

The value of Cs from equivalent nodal load can be described as:

$$C_s = \frac{0{,}5S_1}{\left(\frac{R}{I_e}\right)} = \frac{0{,}5\ .\ 0{,}3539}{\left(\frac{8}{1{,}0}\right)} = 0.022$$

An illustration of computing the drift scale factor for model A can be described as follows:

Cs. W = 0.022 (149728.12) = 3311.80 kN

Vt. Rs_x = 1987,17 kN

Vt. Rs_y = 1987,17 kN

(base shear force from SAP2000 modal /RSA analysis)

According to Article 7.9.1.4.1 of SNI 1726:2019, if the basic shear force resulting from response spectrum modal analysis (Vt) is smaller than Cs.W, then the drift should be multiplied by Cs.W / Vt. According to the aforementioned calculation, the value of Vt = 1987.17 kN, therefore < Cs.W = 3311.80 kN. Consequently, the scale factor for the drift in the x- and y-directions can be expressed in Table 11 as follows:

Scale factor for x-direction=

$$\frac{Cs.W}{Vt\ Rs_y} = \frac{3311{,}80}{1987{,}17} = 1.667$$

Scale factor for y-direction=

$$\frac{Cs.W}{Vt\ Rs_y} = \frac{3311{,}80}{1987{,}17} = 1.667$$

Table 11. Determination of drift scale factor

Parameter	Model A	Model B	Model C	Model D
C_S.W (kN)	3,311.80	3,313.16	3,427.04	3,426.91
$V_T.R_{SX}$	1,987.17	1,711.41	2,046.60	2,155.06
$V_T.R_{SY}$	1,987.17	1,711.41	2,046.60	2,155.06
SF x-dir.	1.667	1.936	1.675	1.59
SF y-dir.	1.667	1.936	1.675	1.59

3.4 Inter-story drift control

Table 12 is the story drift calculation for model A in the x-direction, using the SAP2000 output δ_{xe1}.

Prior to adjusting the limits of inter-story drif design (Δ), the redundancy factor according to SNI 1726: 2019 Article 7.3.4.2. CDC can be categorized in structures as D, E, or F that have a redundancy (ρ) of 1.0 if they satisfy the criteria outlined in SNI 1726:2019. If the moment resistance in the

beam-column connections at both ends of a single beam is lost, the reduction in story strength will not exceed 33% for lateral force resisting elements using MRF.

Table 12. Story drift (model A; SF=1.667; Cd / Ie=5.5)

Story - i^{th}	Drift in story-x / δ_{xe1} (m)	Drift in story - x / δ_{xe2} (m)	Story drift (m)
a	b	e = b . SF.Cd / Ie	f = e_n-e_{n-1}
25	0.079928	0.733	0.007
20	0.073775	0.676	0.018
15	0.062055	0.569	0.027
10	0.045986	0.422	0.033
5	0.026425	0.242	0.040
1	0.007226	0.066	0.066

Table 13. Redundancy calculation.

Story - i^{th}	Section Cut Force (kN)	SCF after plastic hinge (kN)	Differences (%)
25	164.54	162.57	1%
20	745.08	722.55	3%
15	1034.15	1002.93	3%
10	1264.10	1223.88	3%
5	1454.24	1408.44	3%
1	1607.29	1557.21	3%

The section cut in SAP2000 represents the total forces applied to the joints of the frame, shell, and links. The resistance loss at both ends of a single beam, as shown in Table 13, ranges from 1% to 3%, not exceeding 33%. To control story drift, a redundancy factor of 1.0 can be implemented.

Table 14. Story drift control for model A (h_x=3.5m; allowable story drift = 0.07; redundancy=1.0)

Story - i^{th}	Story drift (m)	Δ_{all}/ρ	Status
25	0.007	0.07	satisfy
20	0.018		satisfy
15	0.027		satisfy
10	0.033		satisfy
5	0.040		satisfy
1	0.066		satisfy

Once the redundancy value is established, the subsequent stage involves controlling story drift computed in Table 13. According to SNI code, the four building models are classified under the category of all other structures. Therefore, the allowable story drift for risk category I is 0.020.h_x, where h_x represents the story height. Table 14 is the story drift control for model A.

3.5 Determination of Load Scale

According to SNI 1726:2019 Article 7.9.1.4.1, if the fundamental period of the analysis exceeds CuTa, then the T structural period should be considered as CuTa. The fundamental period in each of the 4 models exceeds the CuTa value in Table 15, hence the structural period is considered as CuTa.

Table 15. Used structural periods of each model

Used Period, (second)			
Model A	Model B	Model C	Model D
3.65	3.65	1.95	1.95

If the total shear force (Vt) obtained from the analysis of variance is less than 100% of the shear force (V) calculated using the equivalent static method, then the force should be multiplied by V / Vt. Table 16 is a simple shear force calculation using the equivalent static method with S_{D1} = 0.3539; S_{DS} = 0.8255; R =8; Ie =1.0; Cs = 0.08.

Table 16. Cs value from each model

Building	Cs	$C_{s\text{-}max}$	$C_{s\text{-}min}$	Used Cs
Model A	0.08	0.016	0.028	0.016
Model B	0.08	0.016	0.028	0.016
Model C	0.08	0.029	0.028	0.029
Model D	0.08	0.029	0.028	0.029

Table 17. Seismic base shear force and scale factors

Items	Model A	Model B	Model C	Model D
Cs	0.016	0.016	0.029	0.029
Weight (kN)	155532	155109	161044	160690
Seismic base shear force V_{base} (kN)	2445.5	2438.8	4728.8	4718.4
Base shear force from modal analysis (kN)	1910.8	1607.3	1971.5	2068.1
Scale factor	1.3	1.5	2.4	2.3
SF input SAP2000	1.6	1.9	2.9	2.8

The calculated C_S value in Table 16 exceeds the value of C_S maximum, hence Cs_{-max} will be controlled the static equivalent base shear force. Table 17 displays the seismic base shear force for each building model.

3.6 Running the software in the stage 1

The structural model will be analyzed using the SAP2000 software to calculate internal forces in order to determine reinforcement requirements. In addition to the previously mentioned loads, SAP2000 software will also incorporate load combinations based on SNI 2847:2019. Building upon the previous loading analysis, the impact of horizontal and vertical seismic forces as outlined in SNI 1726:2019, combination loads 5 and 7 require further elaboration.

1. $(1.2 + 0.2\ S_{DS})\ D + 1.0\ L \pm 1.0\ E_X \pm 0.3\ E_Y$
2. $(1.2 + 0.2\ S_{DS})\ D + 1.0\ L \pm 0.3\ E_X \pm 1.0\ E_Y$
3. $(0.9 - 0.2\ S_{DS})\ D + 1.0\ L \pm 1.0\ E_X \pm 0.3\ E_Y$
4. $(0.9 - 0.2\ S_{DS})\ D + 1.0\ L \pm 0.3\ E_X \pm 1.0\ E_Y$

The wind loads (W), rain loads (R), and snow loads (S) were excluded from consideration in this paper. The complete load combination inputed in SAP 2000 become:

LC1 = 1.4 D + 1.4 S_D
LC2 = 1.2 D + 1.2 S_D + 1.6 L + 0.5Lr
LC3 = 1.2 D + 1.2 S_D + 0.5 L + 1.6Lr
LC4 = 1.33 D + 1.33 S_D + 0.5 L + 1.0EQx + 0.3EQy
LC5 = 1.33 D + 1.33 S_D + 0.5 L + 0.3EQx + 1.0EQy
LC6 = 1.33 D + 1.33 S_D + 0.5 L – 1.0EQx + 0.3EQy
LC7 = 1.33 D + 1.33 S_D + 0.5 L – 0.3EQx + 1.0EQy
LC8 = 1.33 D + 1.33 S_D + 0.5 L + 1.0EQx – 0.3EQy
LC9 = 1.33 D + 1.33 S_D + 0.5 L + 0.3EQx – 1.0EQy
LC10 = 1.33 D + 1.33 S_D + 0.5 L – 1.0EQx + 0.3EQy
LC11 = 1.33 D + 1.33 S_D + 0.5 L – 0.3EQx – 1.0EQy
LC12 = 0.77 D + 0.77 S_D + 1.0EQx + 0.3EQy
LC13 = 0.77 D + 0.77 S_D + 0.3EQx + 1.0EQy
LC14 = 0.77 D + 0.77 S_D – 1.0EQx + 0.3EQy
LC15 = 0.77 D + 0.77 S_D – 0.3EQx + 1.0EQy
LC16 = 0.77 D + 0.77 S_D + 1.0EQx – 0.3EQy
LC17 = 0.77 D + 0.77 S_D + 0.3EQx – 1.0EQy
LC18 = 0.77 D + 0.77 S_D – 1.0EQx – 0.3EQy
LC19 = 0.77 D + 0.77 S_D – 0.3EQx – 1.0EQy

3.7 Beams and columns reinforcement design

The software application SAP2000 v21.2.0 was employed to compute the necessary reinforcement for beams and columns during the analysis of the outcomes for the four building models. The code SNI 2847:2019 is utilized for the reinforcement computation procedures. For the four building models, Table 18 and 19 show the reinforcement for beams, and Tables 20 and 21 for columns, in the corresponding reinforcement drawing.

Table 18. Typical reinforcement in the beams (Source: Authors).

Building	Beam type	At support		At mid span	
		tension	Comp.	tension	Comp.
Model A	B1-A	6D22	4D22	6D22	4D22
	B2-A	3D19	2D19	3D22	2D22
Model B	B1-B	7D22	5D22	7D22	5D22
	B2-B	3D19	2D19	3D19	2D19
Model C	B1-C	7D19	5D19	3D19	2D19
	B2-C	6D22	4D22	4D22	3D22
	B3-C	6D22	4D22	4D22	3D22
	B4-C	4D19	3D19	3D19	2D19
	B5-C	4D19	3D19	3D19	2D19
Model D	B1-D	7D19	5D19	3D19	2D19
	B2-D	5D19	4D19	4D19	3D19
	B3-D	5D19	4D19	4D19	3D19
	B4-D	3D19	2D19	3D19	2D19
	B5-D	3D19	2D19	3D19	2D19
	B6-D	3D19	2D19	3D19	2D19

The beam's reinforcement details for the in Table 19 based on Table 18 results was obtained. While Table 20 shows the typical reinforcement and columns design results for the four models reinforcement detail of column K1-B in Table 21.

3.8 Pushover Analysis

Once the beam and column reinforcement requirements for each building model have been acquired, the subsequent procedure involves inputting these reinforcement requirements and subsequently executing the static pushover analysis. Fig. 5, 6, 7, and 8 illustrate the pushover analysis outcomes for the displacement of model A, B, C, and D, respectively. The plasticization process in building model A is illustrated in Fig. 5.

Table 19. Reinforcement detail of beam B1-B (Source: Authors).

Reinforcement type	B1-B	
	At the support	At mid span
	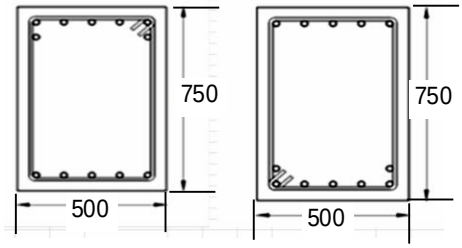	
Upper reinforcement	7D22	5D22
Bottom reinforcement	5D22	7D22
Stirrup shear reinforcement	ϕ12 – 100	ϕ 12 – 150

Table 20. Typical reinforcement in the columns (Source: Authors).

Building Model	Column type	Main reinf.	Shear reinf.	
			support	mid
Model A	K1-A	28D29	ϕ13 – 100	ϕ13 – 150
Model B	K1-B	32D29	ϕ13 – 70	ϕ13 – 100
Model C	K1-C	24D25	ϕ13 – 80	ϕ13 – 150
	K2-C	24D29	ϕ13 – 70	ϕ13 – 100
Model D	K1-D	24D29	ϕ13 – 70	ϕ13 – 100
	K2-D	20D25	ϕ13 – 80	ϕ13 – 100

Table 21. Typical reinforcement detail of column K1-B (Source: Authors).

Reinforcement type	K1-B	
	At support	At mid length
Stirrup shear reinforcement	ϕ13 – 70	ϕ13 – 100
	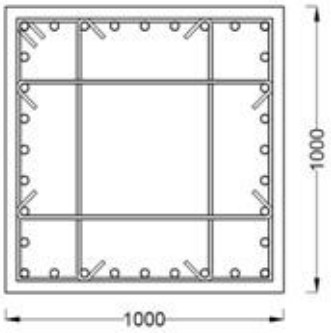	
Column dimension (mm^2)	1000mm x 1000mm	
Main longitudinal reinforcement	32D29	

Step 4 in Fig. 5 provides evidence of the initial post-elastic behavior of the structure, as indicated by the presence of plastic hinges on the beam at level B. Subsequently, commencing from step 5 (not shown), a beam is present at level IO located at the lowermost part of the structure, exhibiting upward propagation as the steps progress. In step 11 (not shown), the lower beam of the structure is positioned at level C. Subsequently, in step 17 (in Fig. 5), the next block's lower portion is situated at level E, exhibiting a deformation of 1,495.75 mm and a sliding base style with a magnitude of 16,370.02 kN.

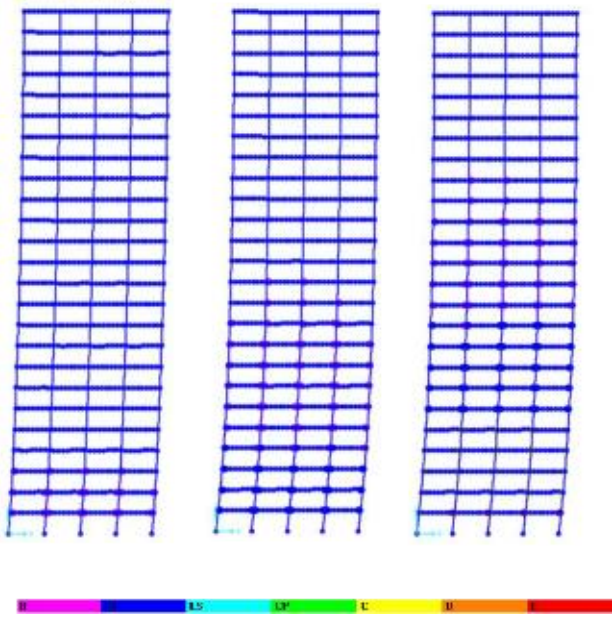

Fig. 5. Pushover analysis deformation and plasticization results of model A in several steps.

Step 4 in Fig. 6 provide evidence of post-elastic behavior in the structure, indicated by the presence of plastic hinges forming on the beam at level B. Next, advance to step 6 (not shown), which involves the identification of a beam located at level IO within a lower structure.

Step 11 (not shown) depicts the beam bottom structure at level C, while steps 19 (in Fig. 6) illustrate the beam bottom structure at level E, exhibiting a deformation of 1,448.01 mm and a base shear force of 11,239 kN. The plasticization process for constructing model C, as depicted in Fig. 7, will now be elucidated.

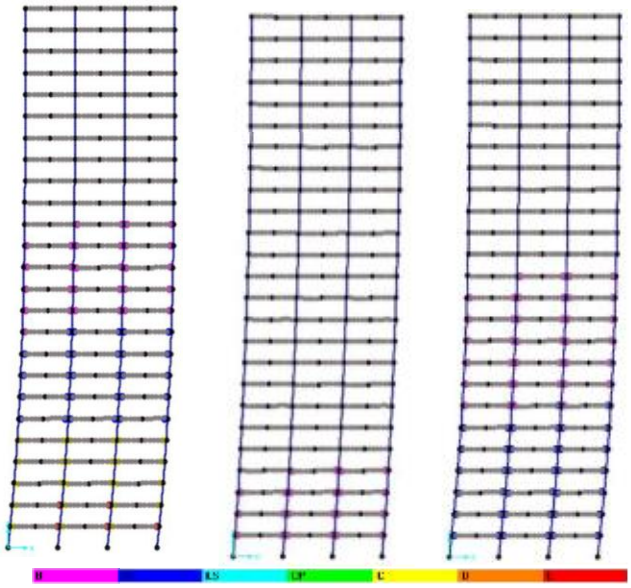

Step 4 Step 10 Step 19

Fig. 6. Pushover analysis deformation and plasticization results of Model B in several steps.

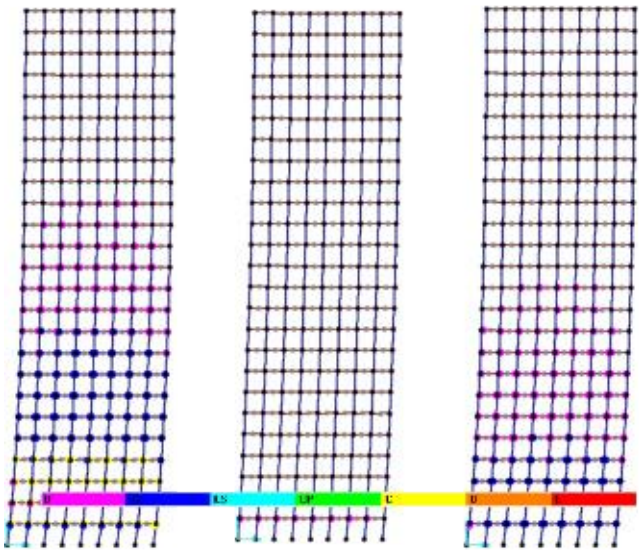

Fig. 7. Pushover analysis deformation and plasticization results of Model C in several steps.

Steps 4-6 in Fig. 7 provide evidence of post-elastic behavior exhibited by the structure, as indicated by the presence of plastic hinges formed on the beam at level B. Subsequently, commencing from step 7 (not shown), a beam is present at level IO located at the foundation of the structure, and it extends vertically as the steps progress. In step 11 (not shown), the lower beam of the structure is positioned at level C. Subsequently, in step 14 (not shown), the lower column commences its placement at level B and continues until step 18 (in Fig. 7), where the lower column reaches level IO, deforms as 1,561.65 mm, accompanied by a base shear force of 22,603 kN.

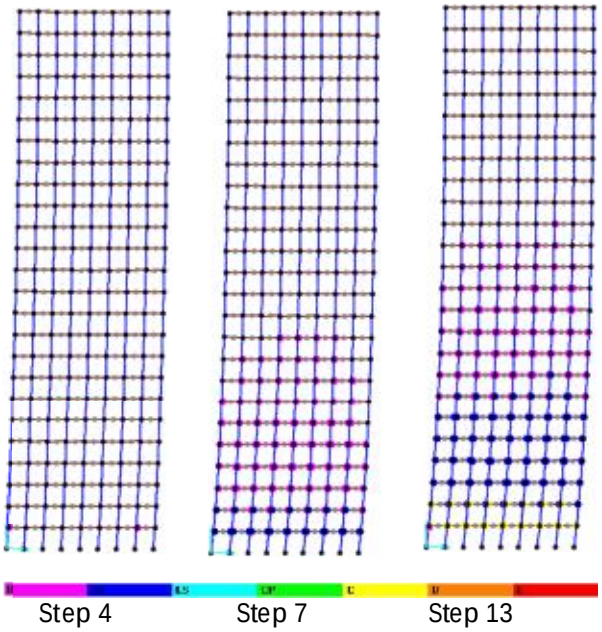

Step 4 Step 7 Step 13

Fig. 8. Pushover analysis deformation and plasticization results of Model D in several steps.

Steps 4 in Fig. 8 provide evidence of post-elastic behavior, which is indicated by the presence of plastic hinges formed on the beam at level B. Next, step 6 (not shown), which involves the identification of a beam located at level IO within a lower structure.

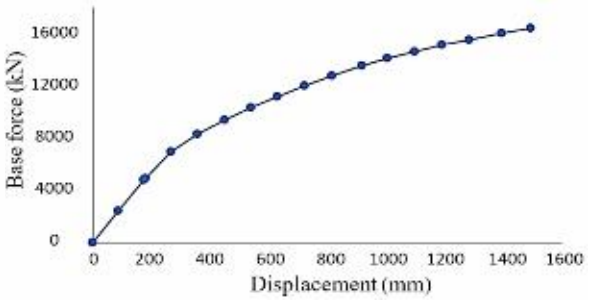

Fig. 9. Capacity curve of Model A.

The lowermost point of the structure on the beam at step 10 (not shown) is situated at level C. From there, it progresses upward to step 13 (in Fig. 8), exhibiting a deformation of 1,065.75 mm and a base shear force of 20,974 kN.

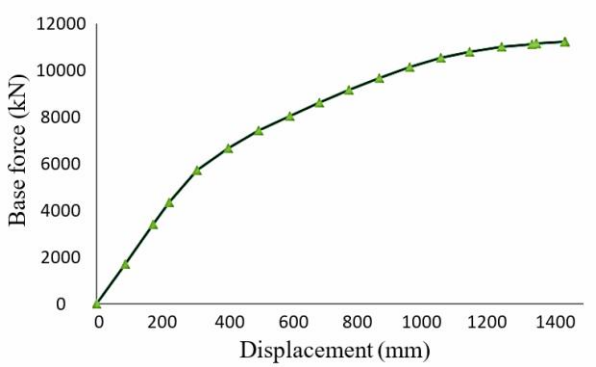

Fig. 10. Capacity curve of Model B.

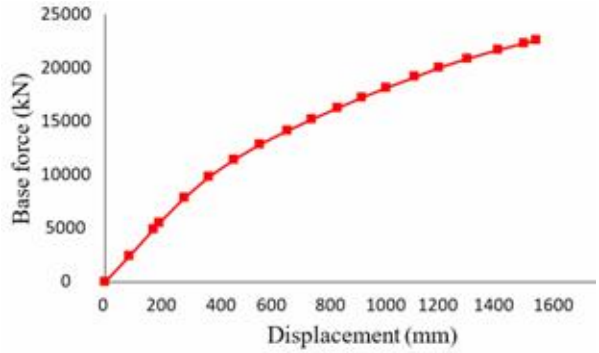

Fig. 11. Capacity curve of Model C.

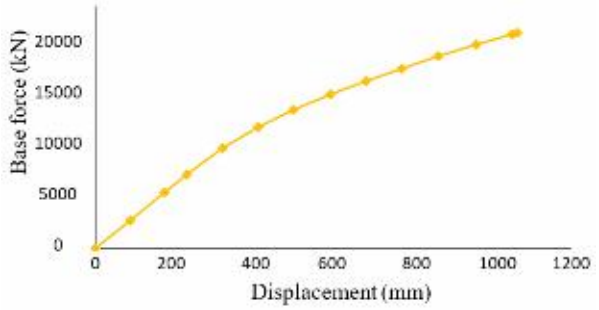

Fig. 12. Capacity curve of Model D.

The direction-xx acquired a 17-step pattern of burden push from the outcomes of conducting static pushover analysis, which was applied to structures until they experienced collapse. Fig. 9 depicts the graphical representation of the correlation between the forces exerted on the structure and its corresponding displacement. This curve serves as a visual representation of the structure's capacity to undergo deformation. The connection style and displacement on model B structure are illustrated in Fig. 10. In the context of model building, it can be observed that in Fig. 11, an 18-step pattern involving the pushing of burdens is implemented. Additionally, a 13-step pattern is applied to the structure depicted in Fig. 12, resulting in its collapse.

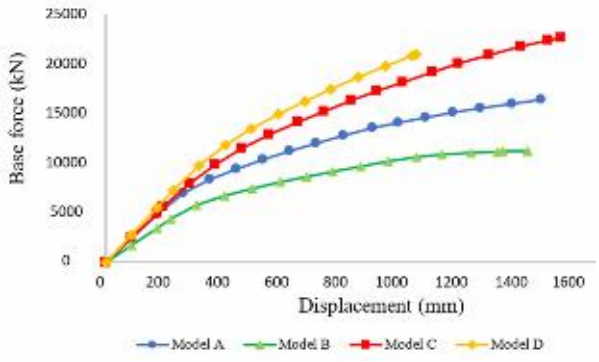

Fig. 13. The capacity of the four building models.

Plastic hinges are observed to develop within the beams located on the lowest floor, and subsequently progress in an upward direction as the magnitude of the thrust load acting upon the structure escalates. After the plastic joints have been formed on the element beam, the process of forming plastic hinges at the base of the basement column should be continued until the structural collapse occurs. Fig. 13 illustrates the capacity curve encompassing all building models.

Fig. 13 illustrates that the initial collapse structures of all building models exhibit a similar degree of displacement. However, the maximum base force is observed in building models C and D, specifically in a framed tube model system.

3.9 Performance Evaluation

The result or consequence of an individual or entity's ability or capacity to perform a particular task or achieve a specific goal. The pushover analysis will employ the capacity method spectrum ATC-40. The approach employed in this study involved generating a demand response spectrum and representing it alongside the curve capacity in a unified format. The concept of

intersection refers to the point or region where two or more entities, such as in the context of spectrum demand and spectrum capacity, the term "point performance" or "performance points" is commonly utilized as depicted in Fig. 14. Identify the period at which the demand spectrum intersects the capacity spectrum within the allowed tolerance. This intersection point in Fig. 14 is considered the performance point.

Fig. 14 used to ascertain if the demand spectrum intersects the capacity spectrum within the permitted tolerance range for each model A, B, C and D, one must compare the demand and capacity spectra at different periods (T).

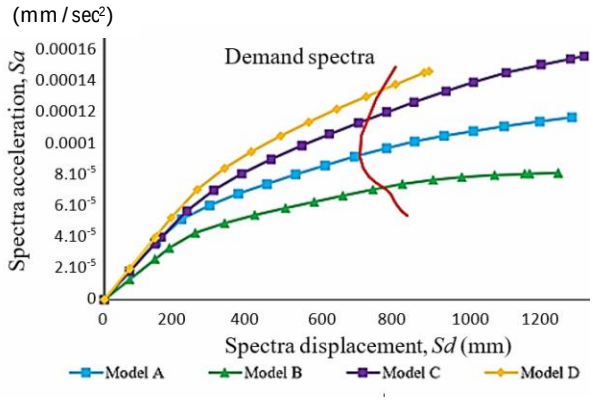

Fig. 14. ATC-40 spectrum capacity of all models.

The demand and capacity spectra are usually represented on a capacity-demand (C-D) curve such as depicted in Fig. 15 to 18. The performance point is defined by the intersection of the two curves within the stated tolerance. The displacement at this position indicates the highest expected displacement for the reference earthquake. It is important to evaluate the structure's performance thoroughly by considering the complete spectrum rather than simply isolated points, over various periods. The objective is to ensure that the building can endure seismic forces within acceptable thresholds.

Fig. 14 illustrates that the initial yield of the structure is observed at a similar displacement level across all building models which the details depicted in Fig. 15 to 18. However, the highest base force is exerted on building models C and D, which are equipped with a framed tube system.

According to Fig. 14, each building model (as depicted in Fig. 15 to 18) exhibits a recognized performance point. Subsequently, performance points were examined to ensure precision, as depicted in Table 22. In order to assess the performance level of structures, it is necessary to consider the average drift ratio of each floor within a building.

This parameter is particularly important when evaluating buildings of varying heights, with the total height of all building models being 87.5 meters. The performance level of each building model is displayed in Table 23.

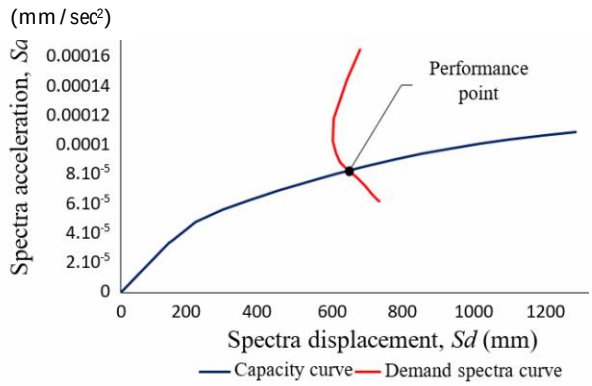

Fig. 15. Spectrum capacity of model A.

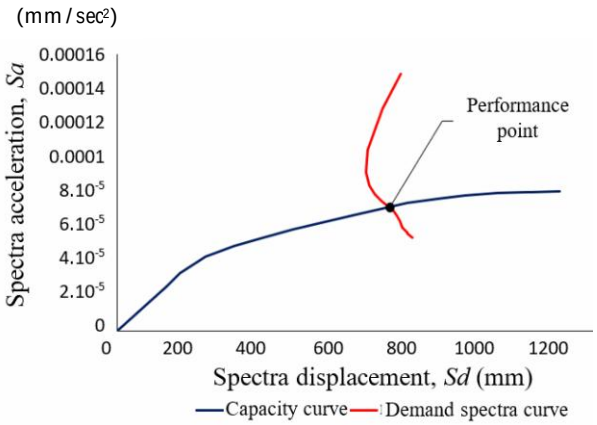

Fig. 16. Spectrum capacity of model B.

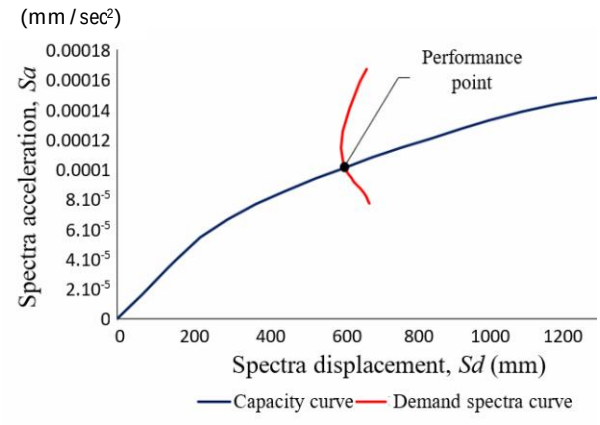

Fig. 17. Spectrum capacity of model C.

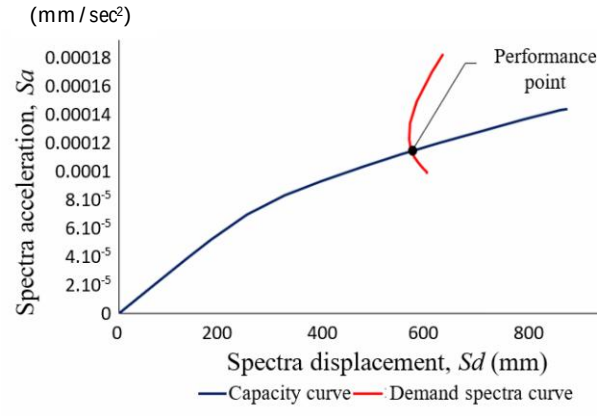

Fig. 18. Spectrum capacity of model D.

Table 22. Performance points (Source: Authors).

Building Model	Performance points	
	V (kN)	D (mm)
Model A	12,330.97	765.43
Model B	9,857.29	906.54
Model C	15,264.96	753.22
Model D	16,577.18	707.75

Table 23. Structural performance level (Source: Authors).

Building Model	Displacement (m)	Drift ratio	Performance Level
Model A	0.765	0.0087	Immediate Occupancy
Model B	0.907	0.0104	Damage control
Model C	0.753	0.0086	Immediate Occupancy
Model D	0.708	0.0081	Immediate Occupancy

According to the results presented in Table 23, the assessment of performance results using the ATC-40 capacity spectrum method for models A, C, and D in the Immediate Occupancy (IO) category that indicates that these models are capable of withstanding seismic events without experiencing damage or structural failure. This implies that the buildings remain safe and can be occupied following an earthquake. Model B falls under the Damage Control (DC) category, which serves as an intermediary stage between Immediate Occupancy (IO) and Life Safety (LS). This implies that the building remains structurally sound and can withstand the effects of the earthquake. Consequently, the likelihood of human casualties is significantly reduced. The analysis of the drift ratios obtained from each building indicates that model D exhibits the lowest drift ratio, thereby demonstrating the most favorable building performance. According to the consecutive ATC-40 method, the buildings are ranked in the following order: model D, model C, model A, and model B.

3.10 Budgeted cost

Table 24 displays the budgeted cost of beams and columns in each building model.

Table 24. Budgeted cost of beams and columns of each model (Source: Authors).

Building Model	Structural elements	Budgeted cost (IDR)	Total Budgeted cost (IDR)
Model A	Column Beam	5.89 B 6.1 B	11.99 B
Model B	Column Beam	5.22 B 5.59 B	10.82 B
Model C	Column Beam	6.84 B 5.77 B	12.61 B
Model D	Column Beam	8.68 B 5.01 B	13.69 B

According to the data presented in Table 24, it can be observed that buildings employing structural system framed tubes models C and D tend to incur higher costs compared to buildings utilizing system structure frames models A and B such depicted in Fig. 19. In Fig. 19, the utilization of a framed

tube structural system in a model D building has been found to yield optimal structural performance. In contrast, when considering higher-priced system frames, an alternative option with comparable structural performance at a reduced cost can be found in Table 24. For instance, the building model C, employing a framed tube system, presents an opportunity to save 7.86% of the budget compared to the building model D.

4. Conclusions

Based on the conducted pushover analysis and evaluation of structural performance, the present study draws the following conclusions regarding the observed frame structural systems, namely model A and model B, as well as the framed tube systems, specifically model C and model D.

1. Model C features larger columns dimensions located on its outer perimeter, while the columns on its inner perimeter are comparatively smaller. Conversely, Model D exhibits the inverse relationship to Model C in terms of column dimensions;
2. The drift ratio findings obtained from pushover analysis utilizing the ATC-40 capacity spectrum method are either equal to or lower than the prescribed drift limit of 0.02;
3. The superiority of Model D building over other building models is attributed to its significantly smaller drift ratio of 0.0081. The evaluation of the structural performance of each building model using the ATC-40 method reveals that models A, C, and D exhibit performance levels classified as Immediate Occupancy (IO);
4. All models are capable of withstanding seismic events without experiencing damage or structural failure. However, model B demonstrates the poorest performance among the models.

5. The limitation of this research

Other researchers and also the authors emphasize the importance of a refined and customized approach to seismic design. They argue that their study offers valuable insights, methodologies, and tools to overcome the constraints of current construction practices that involve rigid floors with flat horizontal reinforced concrete diaphragms, because the rigid diaphragm will not suited well with the assumption made on pushover analysis performance based design.

This design and analysis of real building has a limitation to make a comparison with the experimental setup of a real concrete high-rise building which is nearly impossible and hugely costly. That's why a single full-scale model of Burj Khalifa and another building cannot be found elsewhere. Generally, all were done in an analysis level, due to the structural analysis software has been proven in million cases. A timber or steel miniature is not sufficient as a representative model of a real concrete model due to the scale effect. Therefore it will not prove anything, except in the case of wind-induced building such as flutter, cavitty or vortex analysis, then surely a miniature scale prototype is still needed to be compared with.

REFERENCES

Abdelnaby A. E., Elnashai A. S. (2014), *Performance of degrading reinforced concrete frame systems under the Tohoku and Christchurch earthquake sequences*, Journal of Earthquake Engineering 18(7): 1009-1036, DOI:10.1080/13632469.2014.923796

Ali M. M., Moon K. S. (2018), *Advances in structural systems for tall buildings: emerging developments for contemporary urban giants*, Buildings 8(8): 104, DOI:10.3390/buildings8080104

Arroyo O., Liel A., Gutiérrez S. (2017), *Performance based assessment of reinforced concrete frames designed using eigenfrequency optimization*, Procedia Engineering 199: 3504-3509, DOI:10.1016/j.proeng.2017.09.498

Dalal S. P., Dalal P. (2021), *Strength, deformation and fragility assessment of reinforced concrete moment resisting frame designed by force based design and the performance based plastic design method for seismic loads*, Structures 29: 1154-1164, DOI:10.1016/j.istruc.2020.11.029

Emre I. H. (2021), *Space efficiency in contemporary supertall office buildings*, Journal of Architectural Engineering 27(3): 04021024, DOI:10.3390/architecture1010004

Fu F. (2018), *Design and analysis of tall and complex structures*, Butterworth-Heinemann, Jordan Hill, Oxfordshire, United Kingdom.

Ferrario M. F. (2019), *Landslides triggered by multiple earthquakes: insights from the 2018 Lombok (Indonesia) events*, Natural Hazards 98(2): 575-592, DOI: 10.1007/s11069-019-03718-w

Hazarika H., Rohit D., Pasha S. M. K., Maeda T., Masyhur I., Arsyad A., Nurdin S. (2021), *Large distance flow-slide at Jono-Oge due to the 2018 Sulawesi Earthquake, Indonesia*, Soils and Foundations 61(1): 239-255, DOI:10.1016/j.sandf.2020.10.007

Hosobuchi M. N., Chigira M., Lim C., Komoo I. (2021), *Geological history controlling the debris avalanches of pyroclastic fall deposits induced by the 2009 Padang earthquake, Indonesia: The sequential influences of pumice fall, weathering, and slope undercut*, Engineering Geology 287: 106104, DOI:10.1016/j.enggeo.2021.106104

Imran I., Siringoringo D. M., Michael J. (2021), *Seismic performance of reinforced concrete buildings with double concave friction pendulum base isolation system: case study of design by Indonesian code*. Structures 34: 462-478, DOI:10.1016/j.istruc.2021.07.084

Jena R., Pradhan B., Beydoun G., Alamri A. M., Sofyan H. (2020), *Earthquake hazard and risk assessment using machine learning approaches at Palu, Indonesia*, Science of the Total Environment 749: 141582, DOI:10.1016/j.scitotenv.2020.141582

Liang W., Yang M. (2019), *Urbanization, economic growth and environmental pollution: Evidence from China*, Sustainable Computing: Informatics and Systems 21: 1-9, DOI:10.1016/j.suscom.2018.11.007

Lin K., Lu X., Li Y., Guan H. (2019), *Experimental study of a novel multi-hazard resistant prefabricated concrete frame structure*, Soil Dynamics and Earthquake Engineering 119: 390-407, DOI:10.1016/j.soildyn.2018.04.011

Marinković M., Butenweg C. (2019), *Innovative decoupling system for the seismic protection of masonry infill walls in reinforced concrete frames*, Engineering Structures 197: 109435, DOI:10.1016/j.engstruct.2019.109435

Moosavi S. M. A., Mirhoseini R. T., Kebriaie M. (2022), *Investigation of seismic behavior of the reinforced concrete wall-frame system on a flexible bed*, Results in Engineering 15: 100581, DOI:10.1016/j.rineng.2022.100581

Muljati I., Lumantarna B., Intan R. P., Valentino A. (2017), *Performance of direct displacement based design on regular concrete building against Indonesian response spectrum*, Procedia Engineering 171: 1019-1024, DOI: 10.1016/j.proeng.2017.01.438

Muljati I., Asisi F., Willyanto K. (2015), *Performance of force based design versus direct displacement based design in predicting seismic demands of regular concrete special moment resisting frames*, Procedia Engineering 125: 1050-1056, DOI:10.1016/j.proeng.2015.11.161

Ouyang X., Zhang Y., Ou X., Shi Y., Liu S., Fan J. (2022), *Seismic fragility analysis of buckling-restrained brace-strengthened reinforced concrete frames using a*

performance-based plastic design method, Structures 43: 338-350, DOI:10.1016/j.istruc.2022.06.032

Rahgozar P. (2020), *Free vibration of tall buildings using energy method and Hamilton's principle*, Civil Engineering Journal 6(5): 945-953, DOI:10.28991cej-2020-03091519

Razavi N., Gholizadeh S. (2021), *Seismic collapse safety analysis of performance-based optimally designed reinforced concrete frames considering life-cycle cost*, Journal of Building Engineering 44: 103430, DOI: 10.1016/j.jobe.2021.103430

Reynolds J., Ibáñez-Álamo J. D., Sumasgutner P., Mainwaring M. C. (2019), *Urbanisation and nest building in birds: a review of threats and opportunities*, Journal of Ornithology 160(3): 841-860, DOI:10.1007/s10336-019-01657-8

Rochman T., Rasidi N., Sumardi, Evi N. C., Priyanto A. (2020), *The Effect of Columns Configuration on High-rise Building Using Performance-based Design*, Civil Engineering and Architecture 8(6): 1144-1166, DOI:10.13189/cea.2020.080601

Sarcheshmehpour M., Estekanchi H., Moosavian H. (2020), *Optimum seismic design of steel framed-tube and tube-in-tube tall buildings*, The Structural Design of Tall and Special Buildings 29(14): e1782, DOI:10.1002/tal.1782

Sattar S. (2018), *Evaluating the consistency between prescriptive and performance-based seismic design approaches for reinforced concrete moment frame buildings*, Engineering Structures 174: 919-931, DOI:10.1016/j.engstruct.2018.07.080

Shariati M., Ghorbani M., Naghipour M., Alinejad N., Toghroli A. (2020), *The effect of RBS connection on energy absorption in tall buildings with braced tube frame system*, Steel and Composite Structures, an International Journal 34(3): 393-407, DOI:10.12989/scs.2020.34 .3.393

Shaw B. J., van Vliet J., Verburg P. H. (2020), *The peri-urbanization of Europe: A systematic review of a multifaceted process*, Landscape and Urban Planning 196: 103733, DOI:10.1016/j.landurbplan.2019.103733

Shooli A. R., Vosoughi A., Banan M. R. (2019), *A mixed GA-PSO-based approach for performance-based design optimization of 2D reinforced concrete special moment-resisting frames*, Applied Soft Computing 85: 105843, DOI:10.1016/j.asoc. 2019.105843

Shukla K. P., Dalal S. P. (2017), *Evaluation of response reduction factor of a reinforced cement concrete building designed by performance based plastic design method and limit state design method*, Procedia Engineering 173: 1854-1861, DOI:10.1016/j.proeng.2016.12.235

Sococol I., Mihai P., Petrescu T.C., Nedeff F., Nedeff V., Agop M. (2022), *Analytical Study Regarding the Seismic Response of a Moment-Resisting (MR) Reinforced Concrete (RC) Frame System with Reduced Cross Sections of the RC Beams,* Buildings 12(7): 983, DOI:10.3390/buildings 12070983

Sococol I., Olteanu-Donţov I., Mihai P., Iftode V. I. (2021), *Seismic response of 1/2 scaled two storey reinforced concrete moment resisting frame system using nonlinear static analysis*, IOP Conference Series: Materials Science and Engineering 1141 (1): 012009, DOI:10.1088/1757-899X/1141/1/012009

Syifa M., Kadavi P. R., Lee C.-W. (2019), *An artificial intelligence application for post-earthquake damage mapping in Palu, central Sulawesi, Indonesia*, Sensors 19(3): 542, DOI:10.3390/s19030542

Umar Z., Pradhan B., Ahmad A., Jebur M. N., Tehrany M. S. (2014), *Earthquake induced landslide susceptibility mapping using an integrated ensemble frequency ratio and logistic regression models in West Sumatera Province, Indonesia*, Catena 118: 124-135, DOI:10.1016/j.catena. 2014.02.005

Yu B. (2021), *Ecological effects of new-type urbanization in China*, Renewable and Sustainable Energy Reviews 135: 110239, DOI:10.1016/j.rser.2020.110239

Zameeruddin M., Sangle K. K. (2016), *Review on recent developments in the performance-based seismic design of reinforced concrete*

structures, Structures 6: 119-133, DOI:10.1016/j.istruc.2016. 03.001

Zhang C., Tian Y. (2019), *Simplified performance-based optimal seismic design of reinforced concrete frame buildings*, Engineering Structures 185: 15-25, DOI:10.1016/j.engstruct.2019.01.108

Zhang X., Far H. (2022), *Effects of dynamic soil-structure interaction on seismic behaviour of high-rise buildings*, Bulletin of Earthquake Engineering 20(7): 3443-3467, DOI:10.1007/ s10518-021-01176-z

SNI-1727-2020 (2020), *Beban desain minimum dan kriteria terkait untuk bangunan gedung dan struktur lain* [*Minimum design loads and related criteria for buildings and other structures*], BSN, Jakarta, Indonesia.

Susilo A., Adnan Z. (2013), *Probabilistic seismic hazard analysis of East Java region, Indonesia*, International Journal of Computer and Electrical Engineering 5(3): 341, DOI: 10.7763/IJCEE.2013.V5.728

Received: 20 January 2024 • Revised: 9 March 2024 • Accepted: 11 March 2024